Internalization of annexin A5-functionalized iron oxide particles by apoptotic Jurkat cells

Full Paper

CONTRAST MEDIA & MOLECULAR IMAGING

Received: 25 July 2008, Revised: 5 November 2008, Accepted: 6 November 2008, Published online in Wiley InterScience: 2009

(www.interscience.wiley.com) DOI:10.1002/cmmi.261

Internalization of annexin A5-functionalized iron oxide particles by apoptotic Jurkat cells

Geralda A. F. van Tilborg[a]*, Tessa Geelen[a], Hans Duimel[b], Paul H. H. Bomans[b,c], Peter M. Frederik[b,c], Honorius M. H. F. Sanders[a], Niko M. Deckers[d], Roel Deckers[a], Chris P. M. Reutelingsperger[d], Gustav J. Strijkers[a] and Klaas Nicolay[a]

Apoptosis plays an important role in the etiology of various diseases. Several studies have reported on the use of annexin A5-functionalized iron oxide particles for the detection of apoptosis with MRI, both *in vitro* and *in vivo*. The protein annexin A5 binds with high affinity to the phospholipid phosphatidylserine, which is exposed in the outer leaflet of the apoptotic cell membrane. When co-exposed to apoptotic stimuli, this protein was shown to internalize into endocytic vesicles. Therefore in the present study we investigated the possible internalization of commercially available annexin A5-functionalized iron oxide particles ($r_1 = 34.0 \pm 2.1$ and $r_2 = 205.0 \pm 10.4\ \mathrm{mM^{-1}\,s^{-1}}$ at 20 MHz), and the effects of their spatial distribution on relaxation rates R_2^*, R_2 and R_1. Two different incubation procedures were performed, where (1) Jurkat cells were either incubated with the contrast agent after induction of apoptosis or (2) Jurkat cells were simultaneously incubated with the apoptotic stimulus and the contrast agent. Transmission electron microscopy images and relaxation rates showed that the first incubation strategy mainly resulted in binding of the annexin A5-iron oxide particles to the cell membrane, whereas the second procedure allowed extensive membrane-association as well as a small amount of internalization. Owing to the small extent of internalization, only minor differences were observed between the $\Delta R_2^*/\Delta R_2$ and $\Delta R_2/\Delta R_1$ ratios of cell pellets with membrane-associated or internalized annexin A5 particles. Only the increase in R_1 (ΔR_1) appeared to be diminished by the internalization. Internalization of annexin A5-iron oxide particles is also expected to occur *in vivo*, where the apoptotic stimulus and the contrast agent are simultaneously present. Where the extent of internalization *in vivo* is similar to that observed in the present study, both T_2- and T_2^*-weighted MR sequences are considered suitable for the detection of these particles *in vivo*.

Keywords: apoptosis; annexin A5; iron oxide; internalization; MRI

1. INTRODUCTION

Apoptosis, or programmed cell death, is an essential feature of tissue development and homeostasis. Consequently, deregulation of this form of cell death plays a critical role in the etiology of various disorders, including autoimmune diseases (1), cardiovascular diseases (2) and cancer (3). During the apoptotic process, cells translocate the phospholipid phosphatidylserine (PS) to the outer layer of their cell membranes, which is utilized by surface proteins on macrophages and fibroblasts to recognize and engulf apoptotic cells prior to lysis (4). The protein annexin A5 binds with high affinity ($K_d < 10^{-9}$ M) and specificity to phosphatidylserine in a Ca^{2+}-dependent manner (5), and is therefore considered to be an excellent ligand for targeting apoptotic cells. Fluorescent labeling of this protein has been extensively shown to allow the detection of apoptotic cells with optical imaging techniques both *in vitro* (6) and *in vivo* (7). Similarly, several studies have reported on the use of radiolabeled annexin A5 for the detection of apoptosis in animal models (8) and patients (9) with nuclear imaging techniques. The latter imaging techniques provide a high detection sensitivity, but suffer from a low spatial resolution and lack anatomical information. Therefore several MR contrast agents have been suggested for the detection of apoptotic sites, as MRI provides excellent soft tissue contrast at a relatively high spatial resolution. To overcome the low sensitivity of MRI, most of these contrast agents were targeted iron oxide nanoparticles (10–16), whereas Gd-based nanoparticulate contrast agents have also been proposed (13,17–19).

* *Correspondence to: G. A. F. van Tilborg, Eindhoven University of Technology, NLaag B2.03, Den Dolech 2, 5612 AZ Eindhoven, The Netherlands. E-mail: g.a.f.v.tilborg@tue.nl*

a *G. A. F. van Tilborg, T. Geelen, H. M. H. F. Sanders, R. Deckers, G. J. Strijkers, K. Nicolay*
Biomedical NMR, Department of Biomedical Engineering, Eindhoven University of Technology, The Netherlands

b *H. Duimel, P. H. H. Bomans, P. M. Frederik*
EM-unit, Department of Pathology, Medical Faculty, Maastricht, University Maastricht, The Netherlands

c *P. H. H. Bomans, P. M. Frederik*
Soft Matter Cryo-TEM Research Unit, Department of Biomedical Engineering, Eindhoven University of Technology, The Netherlands

d *N. M. Deckers, C. P. M. Reutelingsperger*
Cardiovascular Research Institute Maastricht, Department of Biochemistry, Maastricht University, The Netherlands

Iron oxide-based contrast agents reduce the intrinsic T_1, T_2 and T_2^* values of tissues with an efficiency that is characterized by the so-called relaxivities r_1, r_2, and r_2^* expressed in $mM^{-1}\,s^{-1}$. In general, iron oxide particles display an r_2/r_1 ratio of >2 at $\geq$20 MHz, which makes these particles most suitable as T_2-reducing agents, i.e. negative contrast agents. The relaxivities of a particular iron oxide particle are determined by a complex interplay between various parameters, including core size, chemical composition, magnetic field strength and spatial distribution. In general, in the range of field strengths used for MRI the r_2 increases, while r_1 decreases with increasing size of the iron oxide core (20). An increase in r_2 was also shown to arise from aggregation of multiple individual iron oxide particles in suspension. This effect on r_2 has been recently exploited in receptor mediated clustering of crosslinked iron oxide particles (CLIO), which allowed the specific detection of oligonucleotides (21) and proteins (22). In contrast, internalization of large numbers of iron oxide particles into confined cellular compartments has been shown to decrease both the r_2 and the r_1 compared with more homogenously dispersed particles (23–26), whereas r_2^* values were found to be increased (25,26). Similar effects were observed *in vivo* when comparing T_1-, T_2- and T_2^*-weighted MR images of the spleen and liver in patients who received SPIO. In these patients, SPIO-induced signal reduction in the liver was most pronounced in T_2^*-weighted images, while T_2 and T_1 effects were most prominent in the spleen. These observations were attributed to differences in numbers and spatial distribution of macrophages in both tissues, resulting in relatively large numbers of small SPIO clusters in the spleen and small numbers of large clusters in the liver (27).

Annexin A5-functionalized CLIO were first presented by Schellenberger *et al*. (10), who demonstrated the ability of this nanoparticle to specifically decrease the signal intensity of camptothecin-treated Jurkat T cells in T_2-weighted images. The fluorescently labeled variant of this nanoparticle allowed the detection of apoptotic cells both with MRI and optical imaging *in vitro* (11) and *in vivo* (12). Bimodal imaging was also enabled by fluorescently labeled micelles with an iron oxide core after covalent coupling of annexin A5 (13). More recently, annexin A5-VSOPs (very small iron oxide particles) were introduced as a novel MR contrast agent for the detection of apoptosis (14). As an alternative to annexin A5, iron oxide particles have also been labeled with the phosphatidylserine-binding C2A domain of the protein synaptotagmin I, which successfully allowed the detection of apoptotic cells both *in vitro* (15) and *in vivo* (16).

All of these studies describe the contrast-generating ability of annexin A5- or synaptotagmin I-functionalized iron oxide particles and their specificity for apoptotic cells. However, little is known about the fate of these contrast agents after binding to their PS target. Recently, it was shown by Kenis *et al*. (28) that fluorescently labeled annexin A5 was internalized into endocytic vesicles by both apoptotic cells and viable tumor cells that express PS. This process is considered to be driven by the formation of two-dimensional crystals of annexin A5 trimers on the apoptotic cell membrane (29). If annexin A5-functionalized iron oxide particles are also internalized into endocytic vesicles, this may affect the T_1, T_2 and T_2^* reducing ability of the contrast agent, which consequently determines the optimal imaging sequence and parameters that should be used for its detection.

The goal of this study was to investigate the possible internalization of annexin A5 iron oxide particles by apoptotic Jurkat cells, and to study the effects of the spatial distribution of these iron oxide particles on different MR parameters. To that aim we compared two different incubation procedures, i.e. the more commonly used binding procedure (10) and the incubation procedure that was shown to lead to internalization of fluorescently labeled annexin A5 (28). Subsequent washing in the presence of Ca^{2+} or in Ca^{2+}-chelating EDTA buffer allowed discrimination between cell membrane associated- and internalized contrast agent.

2. RESULTS

2.1. Contrast agent characterization

Both annexin A5-functionalized and non-functionalized MACS microbeads (Miltenyi Biotec, Auburn, CA, USA) that were originally designed for magnetic cell sorting (32) were applied as T_2-reducing contrast agents. The nanoparticles were composed of an iron oxide core coated with a polysaccharide layer. Cryogenic transmission electron microscopy (cryo-TEM) images of the undiluted non-functionalized microbeads suspension clearly showed the iron oxide core of the nanoparticles, which had an average diameter of 27 ± 6 nm (Fig. 1). Dynamic light scattering (DLS) was used to measure the average hydrodynamic diameter of the non-functionalized and annexin A5-functionalized nanoparticles, which were 75.3 ± 0.7 and 121.0 ± 4.5 nm, respectively.

Relaxivities r_1 and r_2 of the non-functionalized nanoparticles were measured at three different field strengths (0.47, 1.41 and 6.3 T) at room temperature. One should note that only the relaxivities at 6.3 T were acquired in imaging mode, unavoidably using different experimental parameters to those used for relaxivity measurements at 0.47 and 1.41 T. In particular, r_1 was shown to be highly dependent on the field strength, as r_1 decreased from $34.0 \pm 2.1\ mM^{-1}\,s^{-1}$ to $1.0 \pm 0.2\ mM^{-1}\,s^{-1}$ by increasing the field strength from 0.47 to 6.3 T (Table 1). In contrast, r_2 was shown to be less dependent on field strength (Table 1), with r_2 values ranging between $205.0 \pm 10.4\ mM^{-1}\,s^{-1}$ (0.47 T) and $260.7 \pm 8.0\ mM^{-1}\,s^{-1}$ (1.41 T). At 6.3 T, relaxivity r_2 was $222.7 \pm 23.5\ mM^{-1}\,s^{-1}$ (Table 1).

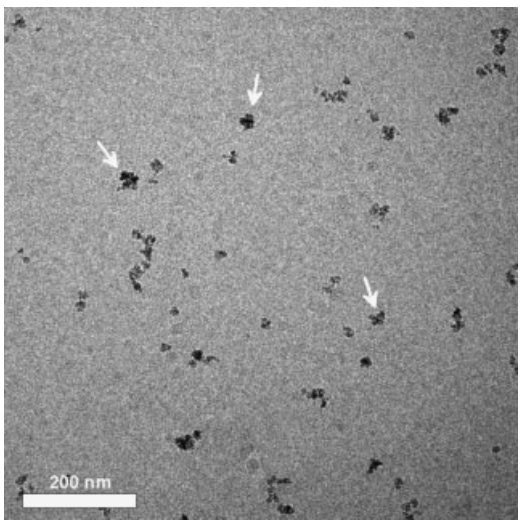

Figure 1. Cryo-TEM image of non-functionalized microbeads at 19,000× magnification. Arrows indicate examples of single microbeads.

Table 1. Relaxivities r_1 and r_2 of the non-functionalized microbeads in HEPES buffered saline at room temperature. Values are expressed per mM Fe

Field strength	r_1 ($mM^{-1}s^{-1}$)	r_2 ($mM^{-1}s^{-1}$)	r_2/r_1 (—)
0.47 T	34.0 ± 2.1	205.0 ± 10.4	6
1.41 T	10.2 ± 0.4	260.7 ± 8.0	26
6.3 T	1.0 ± 0.2	222.7 ± 23.5	223

2.2. Specificity

A T_2-weighted spin echo image ($TR/TE = 5000/40$ ms) of loosely packed pellets of fixed cells, as measured at 6.3 T, showed that the signal intensity of apoptotic cells was drastically lowered after incubation with annexin A5 microbeads compared with apoptotic cells that were left untreated or incubated with basic-microbeads [Fig. 2(A)]. T_2 values within all cell pellets were also quantified and expressed as R_2 relaxation rates, i.e. $1/T_2$. Both cells from the viable and the apoptotic cell population did not show significantly altered R_2 values after incubation with the non-functionalized microbeads compared with untreated control cells [Fig. 2(B)]. R_2 values from the viable cells were non-significantly increased from 18.9 ± 1.8 to $22.2 \pm 3.1\ s^{-1}$ due to incubation with annexin A5 microbeads. In contrast, apoptotic cells that had been incubated with annexin A5 microbeads showed significantly increased R_2 values of $55.2 \pm 7.4\ s^{-1}$ [Fig. 2(B)].

2.3. Variation of apoptotic cell fraction

Cell samples were collected at four different time points after introduction of the apoptotic stimulus to allow the relation between the apoptotic cell fraction and the resulting R_2 values after incubation with annexin A5 microbeads to be studied. During 4 h after addition of the apoptotic stimulus, the apoptotic cell fraction within the cell culture was shown to gradually increase from ~3 to ~61%, as measured by flow cytometry. These cells were subsequently incubated with annexin A5 microbeads for 15 min. The R_2 values of the cells were shown to increase from 20.2 ± 1.6 to $54.0 \pm 6.8\ s^{-1}$ in time. A linear correlation ($R^2 = 0.997$) was found between R_2 values of the cell pellets and the fraction of apoptotic cells with a slope of 0.58 ± 0.06, which is expressed as (s^{-1})/(% apoptotic cells) (Fig. 3).

2.4. Contrast agent internalization

Annexin A5-mediated internalization of the nanoparticles was studied by using two different incubation procedures and two different buffers for subsequent washing. For the first incubation procedure, i.e. the binding procedure, cells were first stimulated to undergo apoptosis. Subsequently, these cells were incubated with the annexin A5-functionalized nanoparticles in Ca^{2+}-containing binding buffer for 15 min. Following incubation with the annexin A5 microbeads the R_2^*, R_2 and R_1 values were found to be significantly increased by approximately 304, 212 and 26% compared with untreated control cells, where cells were washed in the presence of Ca^{2+} [Fig. 4(A–C)]. In contrast, only R_2 values were observed to be significantly increased by the annexin A5 microbeads by 25% compared with untreated control samples when the washing procedure was performed in Ca^{2+}-chelating EDTA buffer [Fig. 4(A–C)].

In the second incubation procedure, i.e. the internalization procedure, the cells were simultaneously incubated with the apoptotic stimulus and the annexin A5 microbeads in Ca^{2+}-containing medium M199. In this case, the annexin A5-functionalized contrast agent was shown to significantly increase the R_2 and R_1 values by approximately 476 and 59% compared with untreated control cells, when cell suspensions were extensively washed in the presence of Ca^{2+} [Fig. 4(E, F)]. Under similar conditions T_2^* values were dramatically decreased and consequently too short to be accurately determined [Fig. 4(D)]. Using the internalization procedure, the annexin A5 microbeads were also shown to significantly increase the R_2^* (113%) and R_2 (81%) values of cells that were extensively washed in Ca^{2+}-chelating EDTA buffer, compared with the corresponding control cells [Fig. 4(D, E)]. In contrast, the R_1 values became similar to those of untreated control samples.

For both the binding and the internalization incubation procedures, no significant differences were observed between R_2^*, R_2 and R_1 values of untreated control cells and cells that were incubated with the non-functionalized particles (Fig. 4).

Apoptotic cell pellets were relatively small (<5 μl). Consequently the absolute amount of Fe present within the pellet

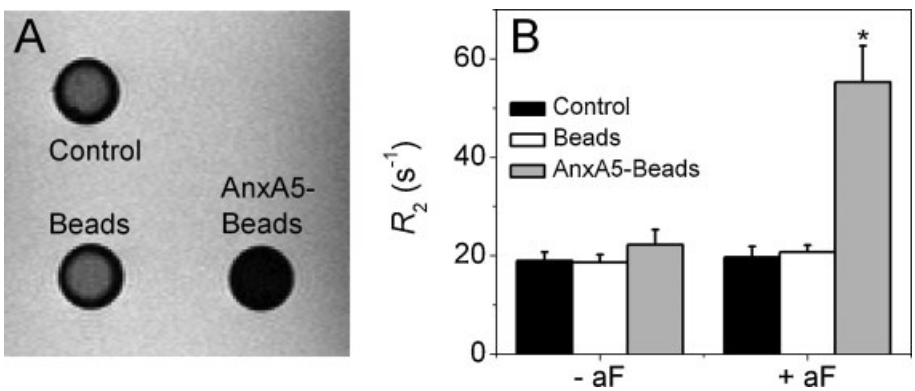

Figure 2. (A) T_2-weighted spin echo image at 6.3 T of fixed apoptotic cell pellets (+ aF) that were untreated (control), incubated with non-functionalized microbeads (beads) or incubated with annexin A5 microbeads (AnxA5-Beads) for 15 min in the presence of Ca^{2+} (0.5 μg Fe/ml). (B) Relaxation rates R_2 of fixed apoptotic (+ aF) and viable (− aF) cell pellets after incubation with the contrast agents (0.5 μg Fe/ml). Untreated cells served as controls. Bars represent mean ± SD, $n = 3$/group. $^*p < 0.05$ relative to the corresponding control cells.

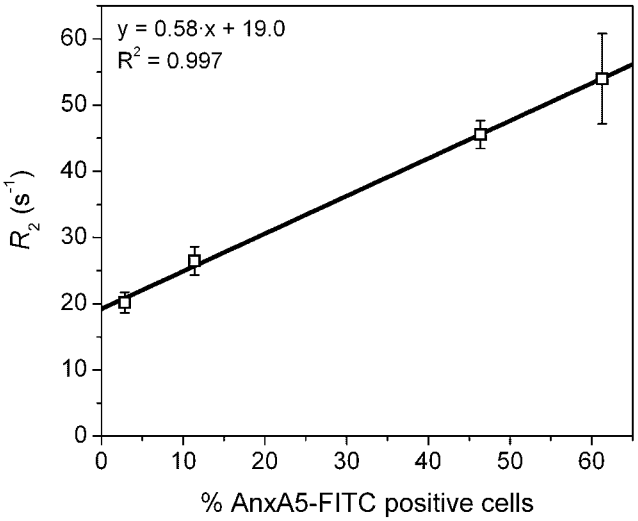

Figure 3. T_2 relaxation rate of anti-Fas treated Jurkat cells that were incubated with annexin A5 microbeads. Annexin A5-FITC labeling was used to determine the percentage of apoptotic Jurkat for each cell sample with flow cytometry.

was relatively low for quantification with for example ICP-MS, and relaxivities could not be determined. Alternatively r_2^*/r_2 and r_2/r_1 ratios were estimated by calculating the differences between the mean relaxation rates of the cell pellets that were incubated with the annexin A5 microbeads and the mean relaxation rates of the corresponding untreated control pellets (ΔR_2^*, ΔR_2, ΔR_1). On the other hand, the r_2^*, r_2 and r_1 values of non-functionalized microbeads in 2.5% glutaraldehyde could be measured, as iron concentrations of the microbeads suspensions were known. However, r_2^*/r_2 and r_2/r_1 ratios of homogeneously distributed particles will be referred to as $\Delta R_2^*/\Delta R_2$ and $\Delta R_2/\Delta R_1$ ratios from now on. Importantly, the $\Delta R_2^*/\Delta R_2$ and $\Delta R_2/\Delta R_1$ ratios of non-functionalized microbeads in 2.5% glutaraldehyde were unaffected by Ca^{2+}. $\Delta R_2^*/\Delta R_2$ ratios of all cell samples, collected either after the binding or internalization procedure, displayed a similar increase compared with $\Delta R_2^*/\Delta R_2$ ratios of dispersed microbeads [Fig. 5(A)]. In contrast, the $\Delta R_2/\Delta R_1$ ratio only appeared to be increased for cells that were co-incubated with annexin A5 microbeads and anti-Fas, followed by removal of the cell-associated microbeads [Fig. 5(B)]. The remaining cell samples all showed $\Delta R_2/\Delta R_1$ ratios equivalent to those observed for dispersed microbeads [Fig. 5(B)].

The apoptotic cell samples that were used for the MR measurements were also examined with electron microscopy to visualize the annexin A5 nanoparticles at the subcellular level. Cell sections were left unstained in order to obtain optimal contrast from only the iron oxide particles in the transmission electron microscopy (TEM) images and to allow subsequent energy dispersion X-ray (EDX) analysis. Consequently, cellular organelles cannot be distinguished, whereas cells and extracellular space can be discriminated. The annexin A5 microbeads present in the cell pellets after extensive washing in Ca^{2+}-containing buffer were found to be located mainly on the outside of the cell membrane when cells were incubated with the contrast agent after the induction of apoptosis, i.e. following the binding procedure [Fig. 6(A)]. In contrast, iron oxide particles were shown to be internalized into endosomal compartments where cells were simultaneously incubated with the annexin A5-functionalized contrast agent and the apoptotic stimulus, followed by washing in EDTA buffer [Fig. 6(B)]. The presence of iron was confirmed by energy dispersive X-ray spectra that were acquired at locations where annexin A5-iron oxide particles were detected on the TEM images (Fig. 7). As expected, no significant amounts of iron were found in surrounding areas where no iron oxides were observed in the

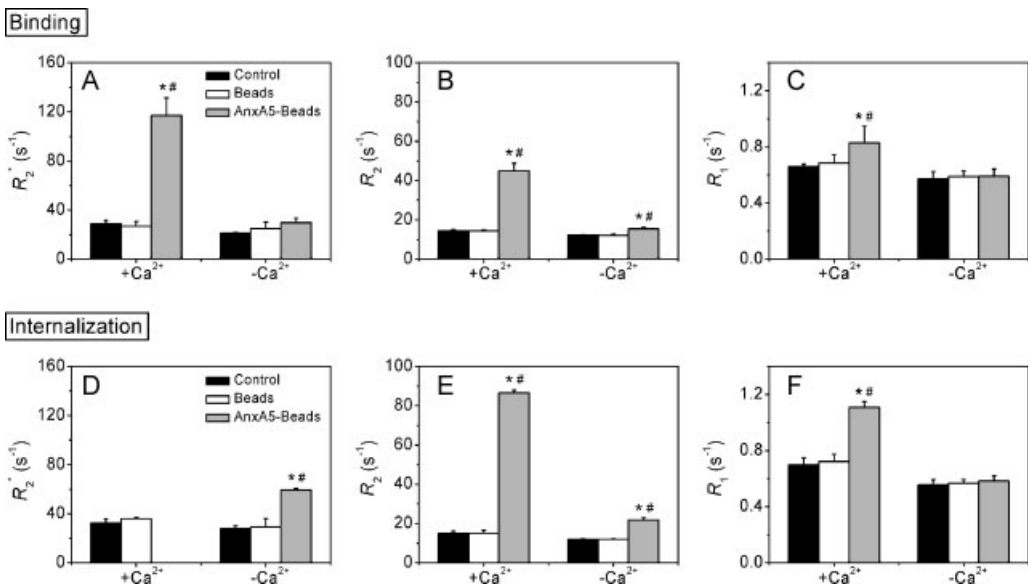

Figure 4. Relaxation rates R_2^* (A, D), R_2 (B, E) and R_1 (C, F) of Jurkat cells that were not treated with microbeads (control), incubated with non-functionalized microbeads (beads) or incubated with annexinA5 microbeads (AnxA5-Beads). Cells were incubated using the binding procedure, i.e. in Ca^{2+}-containing binding buffer after stimulation with anti-Fas (A–C), or using the internalization procedure, i.e. in Ca^{2+}-containing Medium M199 during stimulation with anti-Fas (D–F). Washing was performed in the presence ($+Ca^{2+}$) or absence of Ca^{2+} ($-Ca^{2+}$). T_2^* values of cells that were washed in the presence of Ca^{2+} after simultaneous incubation with AnxA5-Beads and anti-Fas were too low to be measured, and therefore omitted from the figure (D). $^*p < 0.05$ relative to the corresponding control cells. # $p < 0.05$ relative to corresponding cells incubated with non-functionalized microbeads.

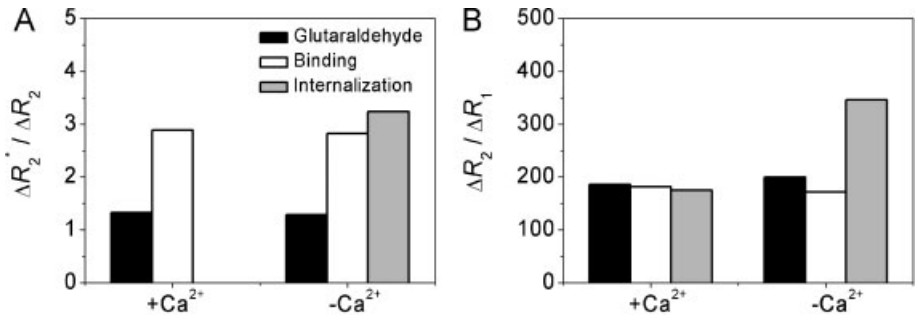

Figure 5. $\Delta R_2^*/\Delta R_2$ (A) and $\Delta R_2/\Delta R_1$ ratios (B) in fixed pellets of apoptotic cells after incubation with annexinA5 microbeads in the binding or internalization experiment. After incubation cells were washed in buffer in the presence ($+Ca^{2+}$) or absence of Ca^{2+} ($-Ca^{2+}$). $\Delta R_2^*/\Delta R_2$ (A) and $\Delta R_2/\Delta R_1$ (B) ratios of homogeneously dispersed non-functionalized microbeads in glutaraldehyde were measured for comparison. No standard deviations are shown as mean R_2^*, R_2 and R_1 values were used for the calculations.

TEM images (Fig. 7). Other elements, including osmium and copper, were both detected in the 'iron oxide area' and the 'surrounding' area as cells were fixed in osmium and placed on copper TEM grids.

3. DISCUSSION

In this study we described *in vitro* studies of a commercially available annexin A5-functionalized iron oxide particle for the detection of apoptotic cells with MRI. T_2-weighted MR images showed a high specificity of these particles for apoptotic Jurkat cells when functionalized with annexin A5, whereas no significant association was observed for non-functionalized microbeads. Schellenberger *et al*. also showed specific reductions in the T_2 values of apoptotic Jurkat cell pellets when incubated with annexin A5-CLIO (0.5 μg Fe/ml) following the standard binding procedure, i.e. by resuspending apoptotic cells in Ca^{2+}-containing binding buffer followed by incubation with the nanoparticles for 10–20 min (10). In the latter study both the fraction of apoptotic cells (~65%) and the increase in R_2 (~153%) were comparable to the values found in our study. Furthermore, annexin A5-functionalized superparamagnetic micelles (13) and annexin A5-VSOP (14) have also been reported to allow the MRI-based detection of apoptotic Jurkat cells using similar incubation protocols. However, significant non-specific association was observed after incubation with M1234-VSOP, i.e. the mutant annexin A5-VSOP that does not bind to PS (14). Such non-specific binding was not observed for non-functionalized CLIO (10), superparamagnetic micelles (13) or the basic microbeads used in the present study. Alternatively, streptavidin-functionalized microbeads were shown to allow the detection of apoptotic EL4 cells in T_2-weighted MR images, through pre-labeling of these cells with the biotinylated C2A domain of synaptotagmin (15).

Compared with most iron oxide contrast agents described in the literature, the microbeads used in this study display a relatively high r_2/r_1 ratio of 6 at 20 MHz (30), which is advantageous for T_2-weighted MR imaging. The particles are not considered to be ferromagnetic, as higher r_2/r_1 ratios would be expected in that case (31). Also, cryo-TEM images showed an inhomogeneous iron oxide core with an average size of 27 ± 6 nm, whereas single crystal sizes of >30 nm are expected for ferromagnetic material (31). The hydrodynamic diameters of the non-functionalized and annexin A5-functionalized particles were 75.3 ± 0.7 and 121.0 ± 4.5 nm, respectively. Consequently the use of these particles for molecular imaging purposes of extravascular targets may be limited by their size.

In most published *in vitro* studies on annexin A5-iron oxides, Jurkat cells were incubated with the contrast agent according to a

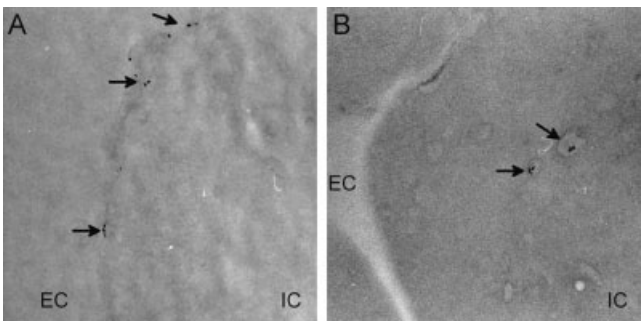

Figure 6. (A) TEM image of an anti-Fas treated Jurkat cell that was subsequently incubated with annexin A5 microbeads for 15 min in Ca^{2+}-containing binding buffer. Extracellular space (EC) can be discriminated from the cytoplasm (IC), indicating that the annexin A5 microbeads (arrows) are bound to the cell membrane (6300×). (B) TEM image of a Jurkat cell that was simultaneously treated with anti-Fas and incubated with annexin A5 microbeads for 3.5 h in $CaCl_2$-containing medium M199 at 37°C and 5% CO_2 in a humidified atmosphere. Subsequent washing was performed in EDTA-containing buffer (8400×).

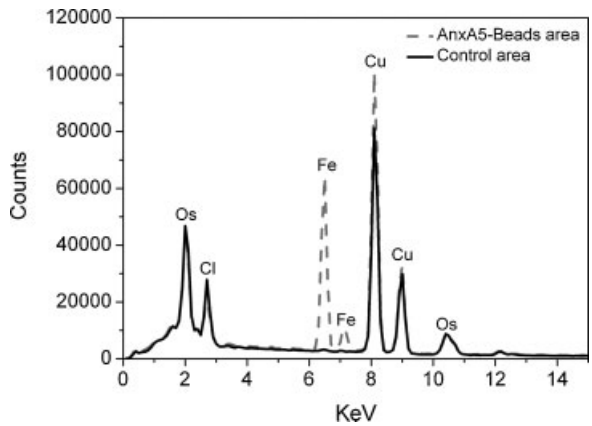

Figure 7. Energy dispersive X-ray spectra acquired in a well-defined area where annexin A5-functionalized iron oxide particles were observed in the TEM images (AnxA5-Beads area) and spectra acquired in an adjacent area where no iron oxides were observed (control area). Osmium (Os), chloride (Cl), iron (Fe) and copper (Cu) were detected.

procedure that is referred to as the standard binding procedure in the present study. During this procedure cells were first treated with an apoptotic stimulus and subsequently incubated with the contrast agent during approximately 10–20 min at room temperature. TEM images that were obtained in this study showed that this procedure leads to binding of the annexin A5 to the cell membrane. These observations were confirmed by MRI of cell pellets, which showed that the obtained increases in R_2^* and R_1 were dramatically reduced, essentially to baseline levels, after removal of Ca^{2+}. Only R_2 remained significantly increased after removal of Ca^{2+}. Nevertheless, in the *in vivo* situation, the apoptotic process and exposure to the contrast agent are likely to occur simultaneously and over a longer time period. Therefore, Jurkat cells were also co-incubated with the apoptotic stimulus (anti-Fas) and the iron oxide particles in Ca^{2+}-containing medium M199. Using this 3.5 h incubation protocol, annexin A5-functionalized microbeads were partially internalized, as shown in TEM microscopy images of Jurkat cells that were washed in Ca^{2+}-chelating EDTA buffer. These results were corroborated by MRI of the corresponding cell pellets, which showed significantly increased R_2^* and R_2 values. Moreover, an additional large fraction of annexin A5-functionalized microbeads appeared to be membrane-associated, as demonstrated by the R_2^*, R_2 and R_1 values that were further increased in the presence of Ca^{2+}.

Internalization of annexin A5 has also been observed for co-incubations of annexin A5-Oregon Green and the apoptotic stimulus anti-Fas (28). The present iron oxide internalization is considered to be completely driven by the binding of annexin A5 to phosphatidylserine on the outer leaflet of the early apoptotic cell membrane, as apoptotic cells neither internalize nor bind non-functionalized microbeads. Whether this annexin A5-dependent internalization of the iron oxide particles is also driven by the formation of two-dimensional crystals of annexin A5 trimers on the apoptotic cell membrane remains to be investigated (28). However, most likely other annexin A5-iron oxide particles are also internalized by apoptotic cells.

Cells with cell membrane-associated iron oxide particles in the presence of Ca^{2+} showed $\Delta R_2^*/\Delta R_2$ ratios that were increased by a factor of 2.2 compared with dispersed non-functionalized microbeads in equivalent fixation solution, whereas $\Delta R_2/\Delta R_1$ ratios were found to remain unchanged. Assuming that the relaxivities of the annexin A5-functionalized and non-functionalized iron oxide particles were similar, the latter observation suggests that there is no restricted water exchange with the iron oxide particles due to pelleting of the cells, as limited water exchange would have resulted in increased $\Delta R_2/\Delta R_1$ ratios. Therefore, the increase in $\Delta R_2^*/\Delta R_2$ probably mainly results from increased ΔR_2^* values due to binding of the iron oxides to the cell membranes of apoptotic cells within the pellet. This reduces Brownian motion of these particles, leading to higher static dephasing gradients. Internalization of the annexin A5 microbeads and removal of membrane-associated contrast agent caused an increase in the $\Delta R_2^*/\Delta R_2$ ratio by a factor of 2.5 compared with dispersed non-functionalized iron oxide particles. Only small differences were observed between the $\Delta R_2^*/\Delta R_2$ ratios of cell membrane-associated and internalized iron oxide, which most likely is due to the small extent of internalization. More extensive internalization of iron oxide particles has been reported to increase the $\Delta R_2^*/\Delta R_2$ ratios by one order of magnitude compared to uniformly distributed iron oxide (25,26). Compartmentalization of the iron oxides limits the access of water, resulting in increased $\Delta R_2/\Delta R_1$ ratios. The small amount of internalized iron oxide particles in the present study only caused a modest increase in the $\Delta R_2/\Delta R_1$ ratio where cells were washed in Ca^{2+}-chelating EDTA buffer, i.e. in the absence of large amounts of membrane-associated contrast agent. At 1.5 T, Billotey *et al*. (23) showed an increase in $\Delta R_2/\Delta R_1$ by a factor of 6.3 after internalization of anionic magnetic particles into endosomes, whereas Simon *et al*. (24) demonstrated an increase by a factor of 1.5 owing to internalization of ferumoxtran-10. In both cases this was due to a relatively large decrease in ΔR_1 with respect to ΔR_2.

The extent to which the T_2 is reduced due to cell-membrane association or internalization of annexin A5-iron oxide particles is determined by the number of apoptotic cells within an imaging voxel. In this study, a linear relation was found between the fraction of apoptotic cells and the transverse relaxation rate R_2, which suggests that annexin A5 microbeads can be used to quantify the level of apoptosis with MRI *in vitro*, when following the standard incubation procedure. Sosnovik *et al*. (12) also demonstrated a linear relation between the percentage of apoptotic cells and the transverse relaxation rate R_2^*, with a slope of 0.4 (s^{-1})/(% apoptotic cells), by mixing viable and apoptotic cardiomyocytes that were incubated with annexin A5-CLIO (1 μg Fe/ml) for 10 min. Whether linearity is maintained when annexin A5-iron oxide particles are internalized by apoptotic cells, which is expected to occur *in vivo*, remains to be investigated.

In conclusion, in the present study we demonstrated specific association of commercially available iron oxides to apoptotic cells. It was shown that cell membrane association partially leads to internalization of the iron oxide particles when co-incubated with the apoptotic stimulus, which is also expected to occur *in vivo*. Based on the $\Delta R_2^*/\Delta R_2$ and $\Delta R_2/\Delta R_1$ ratios, both relaxivities r_2^* and r_2 are probably not strongly affected by the amount of internalization observed in the present study *in vitro*. Therefore, the *in vivo* contrast enhancement in both T_2^*- and T_2-weighted MR images is probably not significantly altered by cellular internalization. Obviously, T_2^*-weighted MR imaging is more sensitive in the detection of iron oxide-based contrast agents. However, as ΔR_2 values are demonstrated not to suffer strongly from iron oxide internalization, both T_2^*- and T_2-weighted imaging sequences are considered suitable for MR molecular imaging of apoptosis when using iron oxide-based contrast agents.

4. EXPERIMENTAL PROCEDURES

4.1. Contrast agent characterization

Cryogenic transmission electron microscopy (cryo-TEM) was performed on an FEI Tecnai 20, type Sphera TEM instrument operating at 200 kV to obtain the mean size of the iron oxide core, using a Gatan cryoholder operating at ∼−170°C. Sample vitrification was carried out using an automated vitrification robot (FEI Vitrobot Mark III).

Dynamic light scattering (DLS) was performed on a Malvern instrument (Zetasizer, Nano-S) to determine the hydrodynamic size of the non-functionalized microbeads in HEPES buffered saline (20 mM HEPES, 135 mM NaCl, pH 7.4), as given by the intensity-weighted particle size distribution. Iron concentrations of the microbead suspensions were measured by atomic absorption spectrometry (Philips, PU 9100X). Prior to the measurements the iron oxide particles were destructed in perchloric acid at 180°C for 1 h, followed by resuspension in 2 ml

ultrapure water. A $Fe(NO_3)_3$ calibration solution (Merck) that underwent the same destruction procedure was used for calibration.

Molar relaxivities ($mM^{-1}\,s^{-1}$) of the nanoparticles were measured at room temperature and different field strengths, i.e. 0.47 T (Bruker, Minispec), 1.41 T (Bruker, Minispec) and 6.3 T (Bruker, Biospec). The non-functionalized nanoparticles were diluted in HEPES buffered saline to final concentrations in the range of 0–0.2 mM Fe. Longitudinal relaxation times T_1 of these samples were obtained using an inversion-recovery sequence, whereas a CPMG sequence was used to determine their transversal relaxation times T_2. For T_2 measurements at 0.47 T and 1.41 T an inter-echo time of 0.1 ms was used, whereas the inter-echo time at 6.3 T was 9 ms.

4.2. Cell culture

The T-lymphoma Jurkat cell line (ATCC) was grown in RPMI1640 medium (Gibco), which was supplemented with 10% fetal calf serum and a mixture of antibiotics, i.e. 100 units/ml penicillin, 0.1 mg/ml streptomycin (Biochrom AG). Cells were grown at 37°C in a humidified atmosphere and 5% CO_2. Apoptosis is naturally occurring without exposing the cells to apoptotic stimuli, typically involving 2.5–10% of the cells within the culture. These cell suspensions are referred to as viable, as the majority of the cells are non-apoptotic.

To induce a high degree of apoptosis, cells were resuspended to 1×10^6 cells/ml supplemented RPMI1640 medium and treated with 200 ng/ml anti-Fas (CD95 human monoclonal antibody, Beckman Coulter B.V.) at 37°C in a humidified atmosphere and 5% CO_2, unless stated otherwise. Following this procedure the cell suspensions are referred to as apoptotic.

Flow cytometry measurements (Coulter EPICS-XL-MCL) were performed to determine the resulting fraction of apoptotic cells in the cell culture. For these measurements 5×10^4 cells were collected and resuspended in binding buffer (2.5 mM $CaCl_2$, 10 mM HEPES, 150 mM NaCl, 5 mM KCl, 1 mM $MgCl_2$) to a final concentration of 1×10^6 cells/ml. Subsequently, annexin A5-FITC was added (250 ng/ml) to label the apoptotic cells and flow cytometry measurements were performed. The resulting data were analyzed in WinMDI 2.8 to determine the fraction of apoptotic cells, by means of (1) forward scatter (FSC) vs side scatter (SSC) plots, and (2) FSC vs fluorescent channel-1 (FL-1) plots. Annexin A5-FITC was measured in FL-1. First, a region of interest (ROI_1) was drawn in the FSC/SSC plots to exclude the apoptotic bodies, which are found in the corner on the left due to their small size. Subsequently FSC/FL-1 plots were obtained, containing only cells from ROI_1. In these plots annexin A5-FITC positive cells could be clearly distinguished from the annexin A5-FITC negative cells. To calculate the fraction of apoptotic cells, the number of annexin A5-FITC positive cells was determined and divided by the total number of cells within ROI_1.

4.3. In vitro targeting

4.3.1. Specificity

The specificity of the annexin A5 microbeads for apoptotic cells and their potential use for MR molecular imaging were investigated. Cells were either grown as usual or the medium was supplemented with anti-Fas for 3 h, in order to induce apoptosis. Subsequently, the cells were harvested and resuspended in Ca^{2+}-containing binding buffer to a final concentration of 2.5×10^6 cells/ml with 5×10^6 cells per sample. Cell suspensions from both the viable and the apoptotic population were incubated with the non-functionalized or the annexin A5-functionalized microbeads for 15 min (0.5 μg Fe/ml), or cells were left untreated. Incubations were performed on a roller bench at room temperature. Following incubation, cells were collected and washed three times (5 min, 300 × ***g***) in binding buffer to remove unbound contrast agents. Next, the cells were fixed in 2.5% glutaraldehyde that was supplemented with 2.5 mM $CaCl_2$. Loosely packed cell pellets were obtained by overnight settling in 250 μl tubes.

4.3.2. Variation of apoptotic cell fraction

Cell suspensions were incubated with annexin A5 microbeads to examine the relation between the fraction of apoptotic cells within the cell culture and the resulting transverse relaxation rate R_2, i.e. $1/T_2$. For this purpose 20×10^6 cells were resuspended in RPMI1640 medium and supplemented with anti-Fas. Next, four cell samples of approximately 5×10^6 cells were collected over a time varying from 0 to 4 h after addition of the antibody. Consequently, each sample was expected to contain a different fraction of apoptotic cells. A total of 5×10^4 cells were taken from each sample to determine the apoptotic fraction with flow cytometry as described above. The remaining cells were resuspended in Ca^{2+}-containing binding buffer (2.5×10^6 cells/ml) and incubated with annexin A5 microbeads for 15 min (0.5 μg Fe/ml) on a roller bench at room temperature. Next, the cells were collected and carefully washed in binding buffer (5 min, 300 × ***g***), followed by fixation and precipitation in 250 μl tubes as described above.

4.3.3. Contrast agent internalization

Two different incubation procedures and two different washing buffers were applied to study the possible annexin A5-induced internalization of the microbeads. The first procedure is the most commonly used incubation procedure to test the target specific interaction of annexin A5-functionalized contrast agents with Jurkat cells, which will be referred to as the binding procedure. In this procedure 5×10^6 cells/sample were first treated for 3.5 h with anti-Fas in RPMI1640 medium, and subsequently these cells were resuspended in 2 ml Ca^{2+}-containing binding buffer to a final concentration of 2.5×10^6 cells/ml. Next, cells were left untreated or incubated with the untargeted- or annexin A5 microbeads on a roller bench at room temperature for 15 min (0.5 μg Fe/ml). During these incubations, cell suspensions predominantly contained cells in the late apoptotic phase. In this phase, annexin A5 mainly shows membrane association without internalization due to reduced membrane dynamics.

Alternatively, in the second procedure, which will be referred to as the internalization procedure, 5×10^6 cells/sample were simultaneously incubated with the apoptotic stimulus (anti-Fas) and the contrast agents at a final concentration of 1×10^6 cells/ml in 5 ml medium M199 (Gibco, Invitrogen), which contained 2 mM $CaCl_2$ and was supplemented with 10% fetal calf serum and a mixture of antibiotics, i.e. 100 units/ml penicillin and 0.1 mg/ml streptomycin (Biochrom AG). The untargeted microbeads (0.5 μg Fe/ml) or annexin A5 microbeads (0.5 μg Fe/ml) were added to the medium directly after addition of the anti-Fas. Samples without addition of the contrast agent served as controls. Incubations were performed on a moving table during 3.5 h, at

37°C in a humidified atmosphere with 5% CO_2. This incubation protocol allowed binding of the annexin A5-functionalized particles during the early apoptotic phase, which is characterized by abundant cell membrane dynamics such as the exposure of PS to the outer leaflet. During this phase, membrane-association of annexin A5 was shown to induce internalization of the protein, driven by the formation of two-dimensional annexin A5 crystals that bend the membrane (28).

Immediately following each incubation procedure all cells were collected and washed three times by centrifugation (5 min, 300 × ***g***) in excessive volumes of Ca^{2+}-containing binding buffer or Ca^{2+} chelating EDTA buffer (5 mM EDTA, 25 mM HEPES, 140 mM NaCl, pH 7.4), in order to remove all non-bound and/or non-internalized contrast agent. Washing in EDTA buffer is expected to remove the phosphatidylserine-associated annexin A5 iron oxides from the cell membrane. Cells that were washed in binding buffer were fixed in 2.5% glutaraldehyde that was supplemented with 2.5 mM $CaCl_2$, whereas the other cells were fixed in 2.5% glutaraldehyde containing 5 mM EDTA. Loose cell pellets were obtained by overnight storage in 250 µl tubes.

4.3.4. *MRI of cell pellets*

MRI measurements were performed at 6.3 T and 20°C (Bruker, BioSpec), using a 3 cm send and receive birdcage coil (Rapid Biomedical). Sets of four samples were placed in the MR scanner, using a home-built sample holder that consisted of a $1.7 \times 1.7 \times 4.8\,cm^3$ water container. Prior to imaging, a $13 \times 13 \times 13\,mm^3$ volume, which included the cell pellets, was shimmed locally. T_2^*, T_2 and T_1 values of the cell pellets were all obtained in single-slice imaging mode, using a slice thickness of 0.7 mm, matrix = 128 × 128 and field of view = 3 × 3 cm^2.

T_2 values were obtained using a Carr–Purcell–Meiboom–Gill (CPMG) sequence, with the following parameters: $TR = 2$ s, $TE = 9$ ms, 32 echoes and number of experiments (NEX) = 8. Apparent T_1 values were measured with a fast T_1 inversion recovery sequence with Fast Low Angle Shot (FLASH) read-out with $TR = 3$ ms, $TE = 1.5$ ms, $\alpha = 15°$, 80 inversion times from 67.5 to 4807.5 ms, NEX = 8 and total repetition time = 20 s. T_1 values were calculated from the apparent T_1 values as described by Deichmann and Haase (33). Additional T_2^* measurements were performed using a single-slice multi-gradient echo sequence with $TR = 2$ s, $TE = 2.6$ ms, $\alpha = 30°$, 32 echoes and NEX = 8.

T_2^*, T_2 and T_1 values of different concentrations (0–2 mM Fe) of non-functionalized microbeads in 2.5% glutaraldehyde, supplemented with either 2.5 mM Ca^{2+} or 5 mM EDTA, were also obtained using similar imaging protocols. From these values, relaxivities r_2^*, r_2 and r_1 were obtained.

4.3.5. *$\Delta R_2^*/\Delta R_2$ and $\Delta R_2/\Delta R_1$ ratios*

Relaxivity measurements within the cell pellets would provide more information on the effect of the spatial localization of the iron oxide particles on the individual relaxivities r_2^*, r_2 and r_1. In general, the relaxivities r_i (r_2^*, r_2 and r_1) of the annexin A5 microbeads can be described by: $\Delta R_i = r_i \cdot$ (AnxA5Beads). In this equation ΔR_i is the difference between the relaxation rates of cell samples that were incubated with the annexin A5 microbeads ($R_{2^*\_AnxA5Beads}$, $R_{2\_AnxA5Beads}$, $R_{1\_AnxA5Beads}$) and the corresponding relaxation rates of untreated apoptotic control cells ($R_{2^*\_pre}$, R_{2_pre}, R_{1_pre}). Obviously, the concentration of annexin A5 microbeads within the cell pellet ([AnxA5Beads]) is required to determine the relaxivities. However, when iron concentrations are below detection limits of analytical techniques, such as inductively coupled plasma mass spectrometry (ICP-MS), the r_2^*/r_2 and r_2/r_1 ratios can be calculated as an alternative, using the following equations:

$$\frac{r_2^*}{r_2} = \frac{\Delta R_2^*}{\Delta R_2} \text{ and } \frac{r_2}{r_1} = \frac{\Delta R_2}{\Delta R_1}$$

These equations hold since both R_2^*, R_2 and R_1 values were measured for each individual cell sample, at consequently identical concentrations of iron.

4.4. Statistics

The mean relaxation times of the cell pellets that were incubated with the annexin A5 microbeads ($n = 3$) were compared with the values found for corresponding untreated control pellets ($n = 3$) and the pellets of cells that were incubated with non-functionalized microbeads ($n = 3$). A one-way ANOVA was applied to the data in Statgraphics Centurion, using Bonferroni's multiple comparison procedure with a 95% confidence level.

4.5. TEM of cells

For transmission electron microscopy (TEM), glutaraldehyde fixed cells were postfixed in 1% osmium tetroxide solution, dehydrated in graded alcohol and embedded in Epon 812. Subsequently, 60 nm slides were cut on a Reichert Ultracut microtome and placed on cupper TEM grids. No further staining was applied to the grids to obtain maximal contrast of the iron oxide particles and to prevent interference of post-staining in the localization of iron (Fe) by energy dispersion X-ray analysis (EDX). EDX enables the specific detection of iron atoms within well-defined areas in the cell, based on element-specific X-ray energy values. TEM images were acquired to study the spatial distribution of iron oxide particles within the cells, using a Philips CM100 electron microscope, operating at 80 kV. EDX spectra were obtained on a Philips CM12 electron microscope, operating at 120 kV and equipped with an EDAX 9900 system. To verify the presence of iron oxide particles, EDX spectra were obtained in small areas where iron oxide particles were considered to be observed on basis of contrast. As a control, EDX spectra were also obtained within surrounding areas where no iron oxides were present.

Acknowledgements

This study was funded in part by the BSIK program entitled Molecular Imaging of Ischemic Heart Disease (project number BSIK03033) and by the EC—FP6-project DiMI, LSHB-CT-2005-512146. This study was performed in the framework of the European Cooperation in the field of Scientific and Technical Research (COST) D38 Action Metal-Based Systems for Molecular Imaging Applications. Furthermore, the authors would like to thank Carmen Burtea from the group of Professor Robert N. Muller from Université de Mons-Hainaut, Belgium for useful discussions on iron quantification.

REFERENCES

1. Carson DA, Ribeiro JM. Apoptosis and disease. Lancet 1993; 341(8855): 1251–1254.

2. Haunstetter A, Izumo S. Future perspectives and potential implications of cardiac myocyte apoptosis. Cardiovasc Res. 2000; 45(3): 795–801.
3. Corsten MF, Hofstra L, Narula J, Reutelingsperger CP. Counting heads in the war against cancer: defining the role of annexin A5 imaging in cancer treatment and surveillance. Cancer Res. 2006; 66(3): 1255–1260.
4. Fadok VA, de Cathelineau A, Daleke DL, Henson PM, Bratton DL. Loss of phospholipid asymmetry and surface exposure of phosphatidylserine is required for phagocytosis of apoptotic cells by macrophages and fibroblasts. J. Biol. Chem. 2001; 276(2): 1071–1077.
5. Gerke V, Moss SE. Annexins: from structure to function. Physiol. Rev. 2002; 82(2): 331–371.
6. van Engeland M, Nieland LJ, Ramaekers FC, Schutte B, Reutelingsperger CP. Annexin V-affinity assay: a review on an apoptosis detection system based on phosphatidylserine exposure. Cytometry 1998; 31(1): 1–9.
7. Dumont EA, Reutelingsperger CP, Smits JF, *et al*. Real-time imaging of apoptotic cell-membrane changes at the single-cell level in the beating murine heart. Nat. Med. 2001; 7(12): 1352–1355.
8. Blankenberg FG, Katsikis PD, Tait JF, *et al*. *In vivo* detection and imaging of phosphatidylserine expression during programmed cell death. Proc. Natl Acad. Sci. USA 1998; 95(11): 6349–6354.
9. Hofstra L, Liem IH, Dumont EA, *et al*. Visualisation of cell death *in vivo* in patients with acute myocardial infarction. Lancet 2000; 356(9225): 209–212.
10. Schellenberger EA, Bogdanov A Jr, Hogemann D, *et al*. Annexin V-CLIO: a nanoparticle for detecting apoptosis by MRI. Mol. Imag. 2002; 1(2): 102–107.
11. Schellenberger EA, Sosnovik D, Weissleder R, Josephson L. Magneto/Optical annexin v, a multimodal protein. Bioconjug. Chem. 2004; 15(5): 1062–1067.
12. Sosnovik DE, Schellenberger EA, Nahrendorf M, *et al*. Magnetic resonance imaging of cardiomyocyte apoptosis with a novel magneto-optical nanoparticle. Magn. Reson. Med. 2005; 54(3): 718–724.
13. van Tilborg GA, Mulder WJ, Deckers N, *et al*. Annexin A5-functionalized bimodal lipid-based contrast agents for the detection of apoptosis. Bioconjug. Chem. 2006; 17(3): 741–749.
14. Schellenberger E, Schnorr J, Reutelingsperger C, *et al*. Linking proteins with anionic nanoparticles via protamine: ultrasmall protein-coupled probes for magnetic resonance imaging of apoptosis. Small 2008; 4(2) 225–230.
15. Jung HI, Kettunen MI, Davletov B, Brindle KM. Detection of apoptosis using the C2A domain of synaptotagmin I. Bioconjug Chem 2004; 15(5): 983–987.
16. Zhao M, Beauregard DA, Loizou L, Davletov B, Brindle KM. Non-invasive detection of apoptosis using magnetic resonance imaging and a targeted contrast agent. Nat. Med. 2001; 7(11): 1241–1244.
17. Prinzen L, Miserus RJJH, Dirksen A, *et al*. Optical and magnetic resonance imaging of cell death and platelet activation using annexin A5-functionalized quantum dots. Nano Lett. 2007; 7(1): 93–100.
18. van Tilborg GA, Mulder WJ, Chin PT, *et al*. Annexin A5-conjugated quantum dots with a paramagnetic lipidic coating for the multimodal detection of apoptotic cells. Bioconjug. Chem. 2006; 17(4): 865–868.
19. Neves AA, Krishnan AS, Kettunen MI, *et al*. A paramagnetic nanoprobe to detect tumor cell death using magnetic resonance imaging. Nano Lett. 2007; 7(5): 1419–1423.
20. Muller RN, Roch A, Colet J, Ouakssim A, Gillis P. Particulate magnetic contrast agents. In The Chemistry of Contrast Agents in Medical Magnetic Resonance Imaging, Merbach AE, Toth E (eds). Wiley: Chichester, 2001; 417–435.
21. Perez JM, Josephson L, Weissleder R. Use of magnetic nanoparticles as nanosensors to probe for molecular interactions. Chembiochem 2004; 5(3): 261–264.
22. Kim GY, Josephson L, Langer R, Cima MJ. Magnetic relaxation switch detection of human chorionic gonadotrophin. Bioconjug. Chem. 2007; 18(6): 2024–2028.
23. Billotey C, Wilhelm C, Devaud M, *et al*. Cell internalization of anionic maghemite nanoparticles: quantitative effect on magnetic resonance imaging. Magn. Reson. Med. 2003; 49(4): 646–654.
24. Simon GH, Bauer J, Saborovski O, *et al*. T1 and T2 relaxivity of intracellular and extracellular USPIO at 1.5 T and 3 T clinical MR scanning. Eur. Radiol. 2006; 16(3): 738–745.
25. Bowen CV, Zhang X, Saab G, Gareau PJ, Rutt BK. Application of the static dephasing regime theory to superparamagnetic iron-oxide loaded cells. Magn. Reson. Med. 2002; 48(1): 52–61.
26. Kuhlpeter R, Dahnke H, Matuszewski L, *et al*. R_2 and R_2^* mapping for sensing cell-bound superparamagnetic nanoparticles: in vitro and murine in vivo testing. Radiology 2007; 245(2): 449–457.
27. Tanimoto A, Oshio K, Suematsu M, Pouliquen D, Stark DD. Relaxation effects of clustered particles. J. Magn. Reson. Imag. 2001; 14(1): 72–77.
28. Kenis H, van Genderen H, Bennaghmouch A, *et al*. Cell surface-expressed phosphatidylserine and annexin A5 open a novel portal of cell entry. J. Biol. Chem. 2004; 279(50): 52623–52629.
29. Oling F, Santos JSDO, Govorukhina N, *et al*. Structure of membrane-bound annexin A5 trimers: a hybrid Cryo-EM—X-ray crystallography study. J. Mol. Biol. 2000; 304(4): 561–573.
30. Wang YX, Hussain SM, Krestin GP. Superparamagnetic iron oxide contrast agents: physicochemical characteristics and applications in MR imaging. Eur. Radiol. 2001; 11(11): 2319–2331.
31. Josephson L, Lewis J, Jacobs P, Hahn PF, Stark DD. The effects of iron oxides on proton relaxivity. Magn. Reson. Imag. 1988; 6(6): 647–653.
32. Dressel R, Elsner L, Quentin T, Walter L, Gunther E. Heat shock protein 70 is able to prevent heat shock-induced resistance of target cells to CTL. J. Immunol. 2000; 164(5): 2362–2371.
33. Deichmann R, Haase A. Quantification of T_1 values by snapshot-flash NMR imaging. J. Magn. Reson. 1992; 96(3): 608–612.